Defects in Semiconductors

Mater. Res. Soc. Symp. Proc. Vol. 1370 © 2011 Materials Research Society
DOI: 10.1557/opl.2011.771

Electronic Structure of O-vacancy in High-*k* Dielectrics and Oxide Semiconductors

Kee Joo Chang[1], Byungki Ryu[1], Hyeon-Kyun Noh[1], Junhyeok Bang[2], and Eun-Ae Choi[3]

[1]Department of Physics, Korea Advanced Institute of Science and Technology, Daejeon 305-701, Korea
[2]Department of Physics, Rensselaer Polytechnic Institute, New York, USA
[3]CAE TEAM, Memory Division, Samsung El. Co., Hwasung, Korea

ABSTRACT

First-principles density functional calculations are performed to investigate the electronic properties of O-vacancy defects in high-*k* HfO_2, Si/HfO_2 interface, and amorphous oxide semiconductors. The role of O-vacancy in device performance is discussed by comparing the results of the GGA, hybrid density functional, and quasiparticle energy calculations.

INTRODUCTION

The technology roadmap reflects that advances in Si-based complementary metal-oxide semiconductor (CMOS) technology will reach the device scale of sub-0.1 μm [1,2]. As the thickness of insulating gate oxide is in the range of 1–2 nm, defects inside oxide and at interface will significantly modify the electrical properties of devices. The use of ultra-thin SiO_2 gate dielectrics leads to a number of problems, such as high leakage current, reduced driving current, reliability degradation, and B penetration [3,4]. For a replacement of SiO_2 gate oxide, HfO_2 has been considered as a promising high-*k* dielectric material, because gate leakage current can be reduced by keeping the same effective oxide thickness [5]. However, this material suffers from a high density of defects, especially O-vacancy, which cause degradation of devices, such as flat band voltage (V_{fb}) shifts, threshold voltage (V_{th}) instability, and low carrier mobility [6,7]. On the other hand, in Hf-silicate based devices, device performance was shown to be greatly improved, with the reduction of threshold voltage shift and instability [8]. The suppression of active trap centers was suggested to be responsible for the reduction of the V_{th} instability [9].

In HfO_2-based devices, V_{fb} shifts were attributed to the Fermi level pinning effect which is caused by interfacial Hf-Si bonds [10] or O-vacancies [11]. In the O-vacancy defect model, the Fermi level pinning is accompanied with a charge transfer between Si electrodes and defects in the oxide, which induces the interface dipole. In theoretical calculations which rely on the local-density functional approximation, defect energy levels cannot be accurately determined because the band gaps are underestimated. Several advanced calculations have been performed for O-vacancy defects in HfO_2 using the screened exact exchange method, the weighted density approximation [12], the hybrid density functional [13-15], and the quasiparticle energy calculations [16]. Despite many studies, the calculated defect levels are quite diverse. Moreover, as the calculations were mostly done for bulk HfO_2, the interface effect on the defect properties was excluded. Recently, theoretical calculations were performed for O-vacancy defects near

Si/HfO_2 interfaces, reporting that O-vacancy defects at the interface can act as electron traps, causing the device instability [17].

Very recently, amorphous oxide semiconductors (AOSs) such as ZnSnO (ZTO) and InGaZnO (IGZO) have attracted much attention because of promising active channel materials for flexible transparent thin-film transistors (TFTs) [18]. AOSs have superior material properties, such as transparency for visible light, flexibility, and low-temperature deposition over large areas [19]. Although the field-effect mobility was reported to be higher by an order of magnitude than that of commercially used hydrogenated amorphous Si [19,20], the device instability is still a challenging issue [21-29]. Among native defects, O-vacancy is considered as a major cause of the degradation of devices [30,31].

In this work we examine the electronic properties of O-vacancy defects in bulk HfO_2 and in Si/HfO_2 interfaces through first-principles density functional calculations. We compare the results of several electronic structure calculations based on the standard density-functional method, the hybrid density functional, and the quasiparticle energy approach for the defect levels and charge transition levels to discuss their role in the performance of high-*k* based devices. Both crystalline and amorphous phases of HfO_2 are used to generate the atomic model for the Si/HfO_2 interface. We also discuss the defect properties of O-vacancy defects in amorphous IGZO semiconductors and their role in the instability of AOS-based TFTs.

THEORY

Our calculations were performed within the density functional theory framework [32]. For O-vacancy (V_O) defects in bulk HfO_2 and Si/HfO_2 interfaces, we first used the generalized gradient approximation (GGA) for the exchange-correlation potential [33] and ultrasoft pseudopotentials [34] for the ionic potentials, as implemented in the VASP code [35]. The wave functions were expanded in plane waves with a cutoff energy of 400 eV. We employed a supercell containing 96 host atoms for bulk HfO_2 and $\sqrt{2} \times \sqrt{2}$ and 2×1 planar supercells for $Si/m\text{-}HfO_2$ and $Si/a\text{-}HfO_2$ interfaces, respectively, where monoclinic and amorphous HfO_2 are placed on the Si (001) surface. We optimized the ionic coordinates and the interface structures until the residual forces were less than 0.05 eV/Å.

The amorphous phase of HfO_2 was generated through the melt-and-quench *ab initio* molecular dynamics (MD) simulations [36]. To model the $Si/a\text{-}HfO_2$ interface, $a\text{-}HfO_2$ was placed on the Si (001) surface, with various thicknesses. Extra O atoms were added to the interface to ensure the insulating interface. A vacuum region of 6.20 Å was inserted at one of the two interfaces to remove the electric field induced by the charge asymmetry between two interfaces, with the surface Si atoms passivated by hydrogen. For the $Si/m\text{-}HfO_2$ interface, we used a repeated slab geometry, which consists of Si and strained $m\text{-}HfO_2$ with 4 unit cells. This interface structure is very similar to the insulating O4 interface between Si and $m\text{-}HfO_2$ [37].

To see the effect of the gap correction on the defect levels and charge transition levels of V_O, we additionally performed both hybrid density functional [38] and quasiparticle energy calculations [39,40]. In the hybrid calculations, the optimized mixing fraction (α) of the Hartree-Fock exchange was estimated to be 0.19 to obtain the measured band gap of $m\text{-}HfO_2$, with the screening parameter of 0.2 cm^{-1}. In the quasiparticle energy calculations, we used the local density functional approximation (LDA) for the exchange-correlation potential and nonlocal pseudopotentials generated by the scheme of Troullier and Martins. Using the Kohn-Sham

energy and wave function, ε_{nk} and Ψ_{nk}, the quasiparticle energy was calculated to first order in the *GW* scheme, which is implemented in the ABINIT code [41],

$$\varepsilon_{nk}(\mathrm{GW}) = \varepsilon_{nk}(\mathrm{KS}) - < \Psi_{nk}(\mathrm{KS}) \mid V_{xc} - \sum_{nk} \mid \Psi_{nk}\,(\mathrm{KS}) >, \quad (1)$$

where V_{xc} and $\sum_{nk}$ (= *iGW*) denote the LDA exchange-correlation potential and electron self-energy operator, respectively, *G* is the Green function, and *W* is the screened Coulomb potential. The first term in Eq. (1) was obtained from the LDA calculations using a 96-atom supercell, which ensures prohibiting interactions between charged defects in supercells. Due to computational demands, the *GW* calculations were done with use of a smaller supercell containing 24 host atoms. As the exchange-correlation potential is less sensitive to the supercell size, numerical errors may not be significant in the second term corrected by the self-energy.

In the GGA and hybrid functional calculations, the charge-transition level $\varepsilon^{q/q-1}$ was directly calculated from the total energies for different charge states q and $q-1$, which is defined as the position of the Fermi level where the charge state of V_O changes, i.e.,

$$\varepsilon^{q/q-1} = E(q-1,q-1) - E(q,q), \quad (2)$$

where $E(q,Q)$ is the total energy of a supercell containing a V_O defect with the actual charge state q and the geometry optimized for charge state Q. On the other hand, in the *GW* approximation, the transition level can be rewritten by adding and subtracting the total energy $E(q-1,q)$ [42],

$$\varepsilon^{q/q-1} = [E(q-1,q-1) - E(q-1,q)] + [E(q-1,q) - E(q,q)]. \quad (3)$$

Here the first term is the atomic relaxation energy (E_r) for the defect charge state $q-1$ between two different geometries optimized for the charge states, q and $q-1$. The second term corresponds to the electron affinity (E_a) or ionization energy (E_i) of V_O in the charge state q with its own optimized structure, which equals the energy of the lowest unoccupied quasiparticle state. The relaxation energy is obtained from the LDA calculations using the 96-atom supercell, whereas the electron affinity or ionization energy is derived from the quasiparticle enegy levels in the *GW* approximation.

DISCUSSION

O-vacancy in HfO_2

The band gaps of *m*-HfO_2 are calculated to be 3.96, 5.72, and 5.87 eV in the GGA, hybrid functional, and *GW* calculations, respectively, as compared to the measured values of 5.6–5.9 eV [43]. In *m*-HfO_2, there exist two types of O-vacancies, $V_{O(3)}$ and $V_{O(4)}$, which are threefold and fourfold coordinated, respectively [figure 1(a)]. The defect levels of $V_{O(3)}$ and $V_{O(4)}$ are compared in figure 2. For the neutral state, the occupied defect levels lie deep in the band gap, regardless of the type of the exchange-correlation potential. In the GGA, $V_{O(3)}$ and $V_{O(4)}$ have the defect levels at 2.71 and 2.29 eV above the valence band maximum E_v (VBM), respectively. Due to the lower defect level, $V_{O(4)}$ is energetically more favorable by about 0.02 eV. With the hybrid density functional, the occupied defect levels with respect to E_v increase to 3.17 and 2.88 eV for $V_{O(3)}$ and $V_{O(4)}$, respectively, while there is a tendency that they decrease in the *GW* approximation.

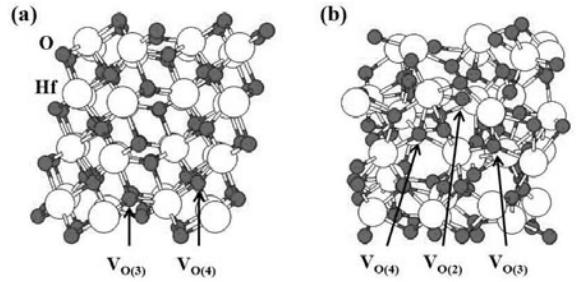

Figure 1. The atomic structures of (a) *m*-HfO_2 and (b) *a*-HfO_2.

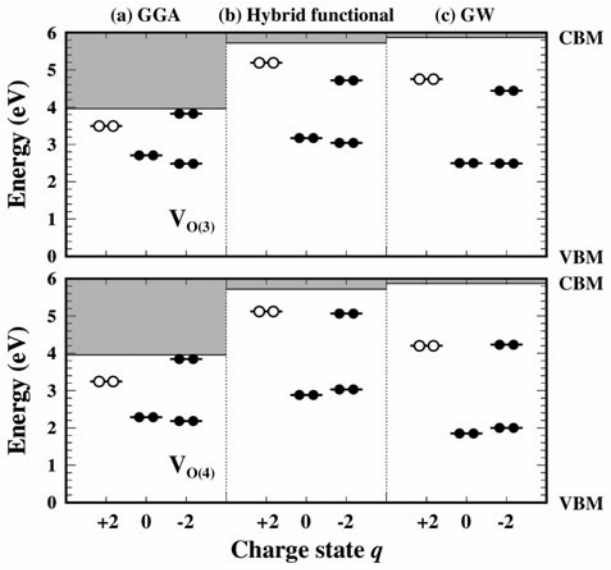

Figure 2. The defect levels for different charge states of $V_{O(3)}$ and $V_{O(4)}$ in *m*-HfO_2: (a) GGA, (b) hybrid density functional, and (c) *GW* (from Ref. 16) calculations.

In the −2 charge state, two electrons occupy the second defect level of V_O. In the GGA, the second defect levels of $V_{O(3)}$ and $V_{O(4)}$ appear at 3.82 and 3.85 eV near the conduction band minimum (CBM). As the occupied defect levels are lower, $V_{O(4)}^{(-2)}$ is also stabilized against $V_{O(3)}^{(-2)}$, similar to the neutral case. When the energy gap is improved with the hybrid density

functional, the second defect levels increase rapidly. However, as their variations are smaller than that of the CBM, the second defect levels are positioned below the CBM, lying at 4.72 and 5.06 eV. In the *GW* approximation, the defect levels are lower but still deep in the gap, being located at 4.44 and 4.23 eV. On the other hand, in the +2 charge state, the defect levels are completely depopulated. Thus, $V_{O(3)}^{(+2)}$ with the higher defect level becomes more stable than $V_{O(4)}^{(+2)}$. While the GGA gives the first depopulated levels at E_v+3.49 and E_v+3.24 eV for $V_{O(3)}^{(+2)}$ and $V_{O(4)}^{(+2)}$, respectively, these levels appear at 5.19 and 5.12 eV in the hybrid density functional and at 4.75 and 4.20 eV in the *GW* approach. Our calculations indicate that the defect level of $V_{O(3)}^{(+2)}$ is in good agreement with the absorption peak which was observed in the energy range 4.5–5.0 eV [44].

The formation energies of $V_{O(3)}$ and $V_{O(4)}$ relative to that of neutral $V_{O(3)}$ are plotted as a function of the Fermi energy for different charge states in figure 3. Three different calculations

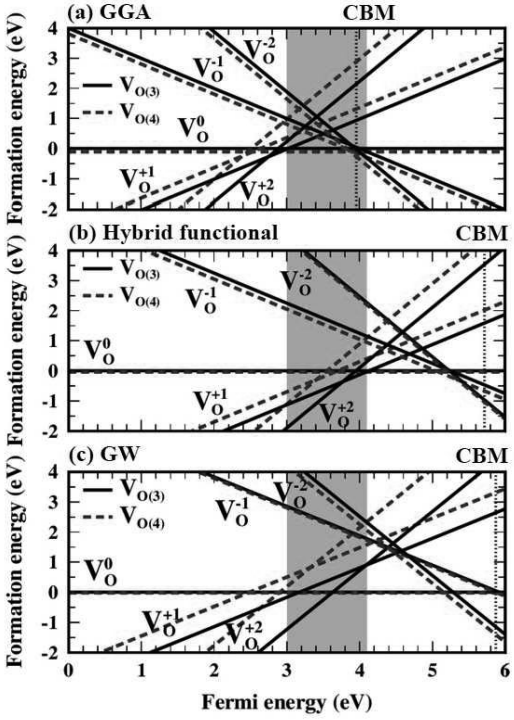

Figure 3. The defect formation energies and charge transition levels of $V_{O(3)}$ and $V_{O(4)}$ in *m*-HfO_2: (a) GGA, (b) hybrid density functional, and (c) *GW* (from Ref. 16) calculations. Shaded areas represent the Si band gap.

give the consistent results for the stability of V_O: $V_{O(3)}$ is more stable for positive charge states, whereas $V_{O(4)}$ is energetically more favorable for neutral and negative charge states. In the GGA calculations, we find that V_O can act as a negative-*U* defect in the electron capture process, with the transition level $\varepsilon^{0/-2}$ at E_v+3.88 eV for $V_{O(4)}$. Although V_O is not the negative-*U* defect for the hole capture, the +1 charge state is only stable on a very narrow window of the Fermi level between 2.76 and 3.02 eV. In the hybrid functional calculations, the behavior of V_O is generally similar to that in the GGA. However, we do not find the negative-*U* behavior, consistent with the previous similar calculations [14]. In this case, the +1 and −1 charge states are also stable in narrow ranges of the Fermi level near 4.0 and 5.2 eV, respectively. If only the neutral and ±2 charge states are considered, the transition levels involving the capture process of two electrons or two holes are $\varepsilon^{+2/0}$ = 3.95 eV for $V_{O(3)}$ and $\varepsilon^{0/-2}$ = 5.22 eV for $V_{O(4)}$, which are higher by about 1.1−1.3 eV than the GGA results. On the other hand, in the *GW* approximation, it is clear that both $V_{O(3)}$ and $V_{O(4)}$ are the negative-*U* defects, with the charge transition levels, $\varepsilon^{+2/0}$ = 3.55 eV for $V_{O(3)}$ and $\varepsilon^{0/-2}$ = 5.04 eV for $V_{O(4)}$. In other calculations using the screened exact exchange potential [12], one transition level $\varepsilon^{+2/0}$ was found at about 4.6 eV, much higher than the hybrid functional and *GW* results.

In HfO_2-based MOS devices, it is known that the V_{fb} shift increases up to 0.2 and 0.5 eV for n^+ and p^+ poly-Si gate electrodes, respectively, with respect to those for SiO_2-based devices [6]. The V_{fb} shift is attributed to the Fermi level pinning effect, which is caused by interfacial Hf-Si bonds and/or O-vacancies. Previous calculations showed that the Fermi level is pinned in the upper Si band in an interface with Hf-Si bonds [10]. As the Hf-Si bonding state is fully occupied, it is difficult to explain the Fermi level pinning, especially in n^+ poly-Si gate electrodes, because the charge transfer cannot occur. On the other hand, it was suggested that the Fermi level can be pinned by a charge transfer between V_O and Si at the interface [11].

In p^+ electrodes, when electrons are transferred from neutral V_O to Si gate, the interfacial dipole induced across the interface raises the Fermi level of Si gate and thereby shifts the flat band voltage. Thus, the pinning level of the Fermi energy can move up to the transition level $\varepsilon^{+2/0}$. In the interface geometry between Si and *m*-HfO_2, the valence band offset is estimated to be about 2.97 eV [17], using the standard reference potential approach [45], whereas the measured values are in the range 2.5−3.5 eV [43,46-47]. In the Si/*a*-HfO_2 interface, the valence band offset is reduced to 2.54±0.30 eV. If the valence band offset of 3.0 eV between Si and *m*-HfO_2 is used,

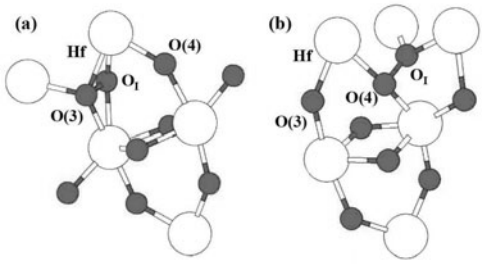

Figure 4. The atomic structures of interstitial O atoms (O_I) bonded to the O(3) and O(4) atoms in *m*-HfO_2, which are threefold and fourfold coordinated, respectively.

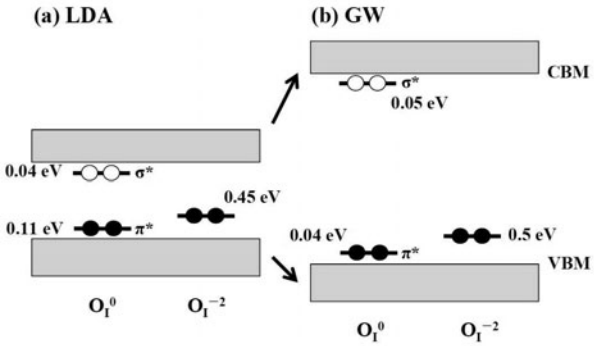

Figure 5. The defect levels of O_I bonded to the O(3) atom in *m*-HfO_2: (a) LDA and (b) *GW* calculations.

the Fermi level can be pinned at the transition level $\varepsilon^{+2/0}$ at 0.55 eV above the Si VBM in the *GW* approximation. This pinning level is in good agreement with experiments [6]. However, in the hybrid density functional, $\varepsilon^{+2/0}$ is positioned at the higher energy of 0.95 eV, close to the Si CBM.

In case of n^+ electrodes, the transition level $\varepsilon^{0/-2}$ is well above the Si band gap in both the *GW* and hybrid density function calculations. Thus, it is difficult to explain the V_{fb} shift in terms of V_O defects in bulk HfO_2. If V_O is in a positive charge state, it can capture electrons from the n^+ electrode and induce the interface dipole, which results in the Fermi level pinning. It is possible for the V_O defect to be positively charged in the presence of acceptors such as oxygen interstitial (O_I). In *m*-HfO_2, an O-interstitial atom is either bonded to the $O_{(3)}$ or $O_{(4)}$ atom, as shown in figure 4. As the O_I-$O_{(3)}$ bond is stronger, the former configuration is lower in energy by 0.8 eV than the latter. In the LDA, two defect levels of neutral O_I lie near the VBM and CBM states, which are denoted as the anti-bonding π* and anti-bonding σ* levels between the two O atoms, respectively. For the $O_I^{(-2)}$ defect, we find one defect level at E_v+0.45 eV. In the *GW* approach, the π* and σ* levels generally follow the variations of the VBM and CBM states, respectively. The defect level of $O_I^{(-2)}$ lies at E_v+0.5 eV, similar to that for $O_I^{(-1)}$ obtained from the screened exact exchange method [12]. Using Eq. (1), we examine the charge transition levels and find that O_I is a negative-*U* defect. Under O-poor growth conditions, O_I becomes more stable than the V_O defect for the Fermi levels higher than 3.5 eV, whereas V_O is energetically more favorable for the Fermi levels below 3.5 eV. Thus, in n^+ poly-Si gate electrodes, the O_I defects can act electron traps, and the Fermi level can be pinned near the CBM.

Very recently, a different defect model was proposed to explain the V_{fb} shift in n^+ poly-Si/HfO_2 gate stacks [17]. At Si/HfO_2 interfaces, the stability and defect levels of V_O are very different from those in the bulk gate oxide due to different local environments. Even in the amorphous phase of HfO_2 [figure 1(b)], the O atoms are mostly threefold or fourfold coordinated, with only the Hf neighbors. The defect levels of V_O far from the interface are not much affected by disorder. In the GGA, we find that the occupied defect levels of neutral V_O defects lie just below the Si VBM, similar to those for $V_{O(3)}$ and $V_{O(4)}$ in the crystalline phase, while the unoccupied levels are positioned near the HfO_2 CBM. In the Si/*a*-HfO_2 interface, as the valence

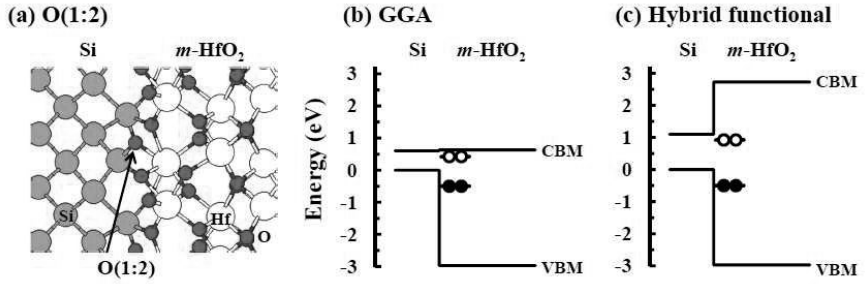

Figure 6. (a) The local geometry around the O(1:2) atom at the Si/*m*-HfO_2 interface, which is surrounded with one Hf and two Si atoms. The defect levels of V_O which is formed at the O(1:2) site: (b) GGA and (c) hybrid density functional calculations (from Ref. 17).

band offset is smaller than that of Si/*m*-HfO_2, the occupied defect levels become closer to the Si VBM. When V_O is formed at or near the interface region, there exists a vacancy site surrounded with both the Hf and Si atoms. If V_O has one Si atom in the neighborhood, the defect level is characterized by the Si dangling bond and lowered by about 0.8 eV, compared with the bulk-like defects. At the Si/HfO_2 interface, we find a peculiar V_O defect with two neighboring Si atoms which form a Si-Si dimer [figure 6(a)] [17]. This dimer bond is weaker than that of the V_O defect in α-quartz. It is interesting to note that the weak dimer bond induces two defect levels different from those of $V_{O(3)}$ and $V_{O(4)}$ in the bulk. While the occupied level is positioned below the Si VBM, the other unoccupied level, which corresponds to the anti-bonding state of the dimer, lies just below the Si CBM [figure 6(b)-(c)]. In the hybrid functional calculations, the anti-bonding level of the weak dimer follows the variation of the CBM with increasing of the optimized mixing fraction α. When the correct band gap is obtained, the charge transition level $\varepsilon^{0/-1}$ is found to lie at about −0.2 eV below the Si CBM. The charge trap level agrees well with the Fermi level pinned in n^+ poly-Si/HfO_2 gate stacks [6].

The V_{th} shifts observed during device operation are also attributed to a high density of charge traps in the interfacial layer or oxide. Thus, the transition levels of V_O are important to explain the origin of the V_{th} instability. The V_{th} instability in *p*MOS devices was shown to be relatively weaker than that in *n*MOS devices [7]. As the defect levels of neutral V_O defects are below the Si VBM, holes can be trapped by neutral $V_{O(3)}$ or $V_{O(4)}$ defects via tunneling through the interface layer when a negative bias is applied in *p*MOS. The hole trap induces the V_{th} instability, and trapped holes can be released by changing gate bias. In *n*MOS, an applied positive gate bias lowers the energy band of the gate oxide. Then, neutral $V_{O(4)}$ defects can trap electrons from the Si channel, becoming $V_{O(4)}^{(-1)}$ or $V_{O(4)}^{(-2)}$. In the hybrid functional, $V_{O(4)}^{(-1)}$ is stable in the oxide band gap, while it is a metastable defect in the *GW* approximation. Regardless of the stability of $V_{O(4)}^{(-1)}$, both the hybrid functional and *GW* calculations show that the electron trap energy, which equals the formation energy difference between $V_{O(4)}^{(0)}$ and $V_{O(4)}^{(-1)}$ with the Fermi level at the oxide CBM, is in the range of 0.1−0.6 eV, as compared to the measured value of 0.35 eV [7]. As the trap energy is small, trap-assisted conduction toward the gate electrode occurs via charge trapping and detrapping in short time scale. At high temperatures, as charge